DALTON
FULL PAPER

Complex chemistry of 2,2,6,6-tetramethyl-4-(2,2′:6′,2″-terpyridin-4′-yloxy)piperidin-1-oxyl, a spin-labelled terpyridine ‡

Malcolm A. Halcrow,*,†,[a] Euan K. Brechin,[b] Eric J. L. McInnes,[c] Frank E. Mabbs[c] and John E. Davies[a]

[a] *Department of Chemistry, University of Cambridge, Lensfield Road, Cambridge, UK CB2 1EW*
[b] *Department of Chemistry, The University of Edinburgh, West Mains Road, Edinburgh, UK EH9 3JJ*
[c] *EPSRC CW EPR Service Centre, Department of Chemistry, University of Manchester, Oxford Road, Manchester, UK M13 9PL*

Reaction of 4′-chloro-2,2′:6′,2″-terpyridine with 4-hydroxy-2,2,6,6-tetramethylpiperidin-1-oxyl in the presence of 4 equivalents of powdered KOH in dmso at 50 °C for 16 h, followed by an aqueous quench, afforded 2,2,6,6-tetramethyl-4-(2,2′:6′,2″-terpyridin-4′-yloxy)piperidin-1-oxyl (L^1) in 70% recrystallised yield. The complexes $[ML^1_2][BF_4]_2$ (M = Mn **1**, Co **2**, Ni **3**, Cu **4** or Zn **5**) have been prepared and characterised. Crystals of **1** grown from MeCN–Et_2O contain octahedral manganese(II) centres, with Mn–N 2.188(3)–2.263(3) Å and Mn · · · N(aminoxyl) distances of 9.740(4) and 9.530(4) Å. The structure shows an unusual O · · · O contact between aminoxyl centres on adjacent molecules. Voltammetric measurements of L^1 and **1**–**5** in MeCN–0.1 M NBu_4PF_6 showed a reversible aminoxyl/oxoammonium oxidation, which is perturbed minimally by complexation; **1**–**4** also showed complex metal-centred redox behaviour, which for **1**–**3** differs from that reported for other $[M(terpy)_2]^{2+}$ derivatives of these metal ions. The X- and Q-band EPR spectra of **4** in MeCN–toluene (10:1) show a broad resonance characteristic of strong Cu/L^1 exchange. Variable temperature susceptibility measurements on solid **1** and **4** revealed weakly antiferromagnetic behaviour. Data for **4** can be reproduced by the Curie–Weiss law, and by an equation describing intramolecular superexchange. However, those for **1** show a sharp drop in $\chi_m T$ below 10 K, which cannot be fitted by these models; it is proposed that this reflects the intermolecular O · · · O contacts in the solid.

Recently, ruthenium(II) complexes of spin-labelled 1,10-phenanthrolines have been used as EPR probes of micellar and dendrimeric macrostructures,[1] and of DNA intercalation.[2] The aminoxyl-substituted phenanthrolines employed in these studies are prepared by three to five step syntheses, requiring high-grade reagents and inert-atmosphere conditions.[3] We report here the high-yield, one-step synthesis of the first spin-labelled terpyridine L^1 from commercially available precursors, which may be of use for these types of application, and as a component of supramolecular devices.[4] The co-ordination chemistry of L^1 with first-row transition ions is also described, with the aim of characterising the electronic and magnetic interactions between the unpaired spins on L^1 and a co-ordinated metal ion.[5]

Results and Discussion

Following a procedure used previously by Constable and Newkome and co-workers[6] for the preparation of 4′-terpyridyl ethers, and recently employed by us to produce L^2,[7] equimolar amounts of 4-hydroxy-2,2,6,6-tetramethylpiperidin-1-oxyl and 4′-chloro-2,2′:6′,2″-terpyridine were allowed to react in dmso in the presence of 4 equivalents of freshly ground KOH at 30 °C; the resultant red solution yielded a pink solid upon addition of water. Recrystallisation from hot hexanes gave L^1 as analytically pure feathery pink needles (Table 1), with reproducible yields of 70–75%.

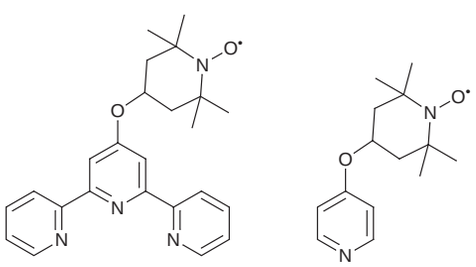

L^1 L^2

The IR spectrum of L^1 as a Nujol mull shows an N–O stretching vibration at 1365 cm^{-1}, while UV/VIS spectroscopy in MeCN shows, in addition to lower wavelength $n \longrightarrow \pi^*$ and $\pi \longrightarrow \pi^*$ bands associated with the 4′-terpyridyl substituent,[8] an aminoxyl $n \longrightarrow \pi^*$ absorption at $\lambda_{max} = 459$ nm ($\varepsilon_{max} = 9.9$ M^{-1} cm^{-1}, Table 2). The X-band EPR spectrum of L^1 in fluid toluene solution shows $\langle g \rangle = 2.006$ and $\langle A(^{14}N) \rangle = 13.6$ G (G = 10^{-4} T). These properties are typical of an aminoxyl radical.[9] The ^{1}H NMR spectrum of L^1 in CD_3CN shows peaks at δ 8.7, 8.3, 7.9 and 7.1 with a 4:2:2:2 integral ratio; this is the expected number of proton environments for the 4′-terpyridyl skeleton, the chemical shifts observed being essentially identical to those shown by diamagnetic 4′-terpyridyl ethers.[6] No broader peaks assignable to the 2,2,6,6′-tetramethylpiperidin-1-oxyl substituent[10] were detected.

Complexation of hydrated $Ni(BF_4)_2$ or $Cu(BF_4)_2$ by 2 molar equivalents of L^1 in MeCN, respectively, affords tan and green solutions from which solid products can be obtained

† *Present address*: School of Chemistry, University of Leeds, Leeds, UK LS2 9JT.

‡ *Supplementary data available*: susceptibility data and fitting procedures for complexes **1** and **4**. For direct electronic access see http://www.rsc.org/suppdata/dt/1998/2477/, otherwise available from BLDSC (No. SUP 57399, 8 pp.) or the RSC Library. See Instructions for Authors, 1998, Issue 1 (http://www.rsc.org/dalton).

Table 1 Analytical and selected FAB mass spectrometric data for the complexes

Compound	Analysis (%)[a] C	H	N	*m*/*z*[b]
L^1	70.4 (71.4)	6.7 (6.7)	13.8 (13.9)	404, 403, 250
1 $[MnL^1_2][BF_4]_2$	55.2 (55.7)	5.3 (5.3)	10.8 (10.8)	862, 707, 552, 458, 303
2 $[CoL^1_2][BF_4]_2$	54.9 (55.5)	5.3 (5.2)	10.8 (10.8)	866, 711, 556, 462, 307
3 $[NiL^1_2][BF_4]_2 \cdot MeNO_2$	53.5 (53.5)	5.3 (5.2)	11.6 (11.5)	865, 710, 555, 461, 306
4 $[CuL^1_2][BF_4]_2$	54.2 (55.2)	5.2 (5.2)	10.5 (10.7)	870, 715, 560, 466, 311
5 $[ZnL^1_2][BF_4]_2 \cdot MeCN$	54.4 (55.2)	5.2 (5.3)	11.4 (11.6)	871, 716, 561, 462, 312

[a] Calculated values in parentheses. [b] Peaks for L^1 are assigned to the ions $[M + H]^+$, $[M]^+$, $[M - C_9H_{17}NO]^+$. Peaks for complexes **1**–**5** are assigned to the ions $[ML^1_2 + H]^+$, $[ML^1(L^1 - C_9H_{17}NO) + H]^+$, $[M(L^1 - C_9H_{17}NO)_2 + H]^+$ and $[M(L^1 - C_9H_{17}NO)]^+$ (M = ^{55}Mn, ^{59}Co, ^{58}Ni, ^{63}Cu or ^{65}Zn).

Table 2 The UV/VIS spectroscopic data for the compounds in this study (MeCN, 293 K)

Compound	Solvent	λ_{max}/nm (ε_{max}/M^{-1} cm^{-1})
L^1	MeCN	212 (sh), 240 (28 000), 276 (23 700), 282 (sh), 307 (sh), 459 (9.9)
1 $[MnL^1_2][BF_4]_2$	MeCN	212 (sh), 245 (58 600), 254 (sh), 274 (53 300), 282 (sh), 311 (24 000), 324 (21 300), 360 (sh), 390 (sh), 445 (sh)
2 $[CoL^1_2][BF_4]_2$	MeCN	246 (60 500), 271 (54 100), 282 (sh), 305 (27 100), 315 (sh), 348 (sh), 452 (966), 500 (715), 540 (sh), 640 (sh)
3 $[NiL^1_2][BF_4]_2$	MeCN	244 (54 100), 268 (sh), 272 (59 500), 298 (sh), 312 (24 700), 325 (19 200), 416 (sh), 495 (sh), 812 (41)
	$MeNO_2$	415 (sh), 490 (sh), 811 (42)
4 $[CuL^1_2][BF_4]_2$	MeCN	228 (sh), 245 (sh), 250 (60 600), 257 (sh), 270 (sh), 312 (23 000), 320 (sh), 445 (sh), 697 (71)
	$MeNO_2$	445 (sh), 695 (71)
5 $[ZnL^1_2][BF_4]_2$	MeCN	213 (sh), 244 (60 100), 251 (sh), 268 (sh), 273 (48 700), 282 (sh), 300 (sh), 310 (28 000), 322 (31 100), 454 (22)

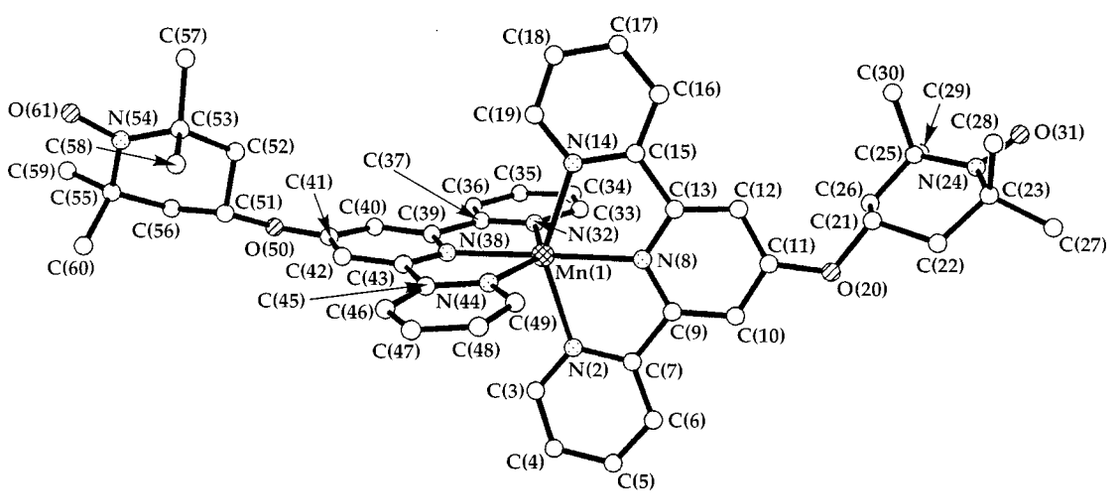

Fig. 1 Solid state structure of the $[MnL^1_2]^{2+}$ dication in complex **1**·1.5MeCN·0.25H_2O, showing the atom numbering scheme employed. For clarity, all hydrogen atoms have been omitted

upon concentration and addition of Et_2O. Similarly, treatment of hydrated $Mn(O_2CMe)_2$, $Co(O_2CMe)_2$ or $ZnCl_2$ with 2 equivalents of L^1 and $NaBF_4$ in MeCN gives yellow (M = Mn), orange (M = Zn) and brick red (M = Co) solid products after filtration and work-up as before. All these compounds were recrystallised from MeCN–Et_2O except the nickel(II) product, which was sparingly soluble in MeCN and hence recrystallised from $MeNO_2$–Et_2O; the recrystallised yields of these reactions were 55–70%. The microcrystalline products desolvated upon drying, and were formulated as the expected complexes $[ML^1_2][BF_4]_2$ by microanalysis (M = Mn **1**, Co **2**, Ni **3**, Cu **4** or Zn **5**; Table 1). This conclusion was confirmed by FAB mass spectrometry, which uniformly showed a highest molecular ion corresponding to $[ML^1_2]^+$ (Table 1).

The IR spectra of complexes **1**–**5** shows peaks arising from L^1 and BF_4^- only. In particular, the ν(N–O) vibration in each of these products occurs at 1366 ± 1 cm^{-1}, suggesting that L^1 is not co-ordinated to these metals through the aminoxyl O atoms. Attempts to prepare oligomeric or polymeric derivatives containing metal ions bridged by L^1 *via* co-ordination of the aminoxyl pendant, by complexation of hydrated MX_2 salts (M = Mn, Co, Ni or Cu; $X^- = MeCO_2^-$, ClO_4^- or BF_4^-) by equimolar or substoichiometric amounts of L^1, afforded in all cases only reduced yields of $[ML^1_2]X_2$.

The L^1 $n \longrightarrow \pi^*$ transition is only clearly resolved in the UV/VIS spectrum of complex **5**, appearing at λ_{max} = 454 nm (ε_{max} = 22 M^{-1} cm^{-1}) in MeCN (Table 2); the intensity of this band is consistent with the proposed stoichiometry of 2 L^1 ligands per molecule. For **4** this peak is visible as a shoulder, while for **1**–**3** it is obscured by a charge-transfer tail. The d-d spectra of **3** and **4** in MeCN and $MeNO_2$ are barely distinguishable (Table 2), suggesting that ligand dissociation from the metal centres does not occur significantly in these solvents, and are essentially identical to those of $[Ni(terpy)_2]^{2+}$ [11,12] and

$[Cu(terpy)_2]^{2+}$ [11,13] in solution. The visible spectrum of **2** has a similar form to that of $[Co(terpy)_2]^{2+}$,[14] showing intense peaks at $\lambda_{max} = 452$ ($\varepsilon_{max} = 966$ M^{-1} cm^{-1}), 500 (715), 540 (sh) and 640 (sh) nm. However, while their maxima lie at very similar wavelengths, the intensities of these bands are only 60–75% of those of the terpy complex. This sensitivity of these absorptions to substitution at the co-ordinated ligand is consistent with previous suggestions that these transitions do not have pure d-d character.[14] The UV spectra of **1**–**5** also exhibit $\pi \longrightarrow \pi^*$ transitions from the terpy framework, close to $\lambda_{max} = 245$ ($\varepsilon_{max} \approx 60\,000$) and 310 nm ($\approx 25\,000$ M^{-1} cm^{-1}).

Single crystal structure

Although complexes **1**–**5** do not crystallise well, vapour diffusion of Et_2O into moderately concentrated solutions of **1** in MeCN was found to yield yellow plates that were suitable for single crystal X-ray analysis. A view of the complex dication is shown in Fig. 1, while selected metric parameters from the structure are listed in Table 3.

The manganese(II) ion adopts the expected octahedral co-ordination with Mn–N distances in the range 2.188(3)–2.263(3) Å, showing a tetragonal compression of 0.06 Å along the molecular z axis. The bond lengths and angles at Mn(1) are crystallographically indistinguishable from those in the published structure of $[Mn(terpy)_2][I_3]_2$.[15] According to the structural indices of Figgis *et al.*[16] for terpy complexes, the average N···N···N angle between the N donors of each L^1 ligand 'θ' = 109.7°, the average intraligand N–Mn–N angle 'α' = 72.4° and the 'bite' of L^1 ($2 \sin \frac{\alpha}{2}$) is 1.18. This latter parameter decreases linearly with lengthening average metal–nitrogen distance, the value for L^1 here being in good agreement with this correlation. The N–O bond lengths within the piperidine pendant groups are typical of aminoxyl radicals [N(24)–O(31) 1.284(5), N(54)–O(61) 1.281(5) Å],[9] while both piperidinoxyl rings have the expected chair conformation with the ether substituents occupying an equatorial position. The distances from the aminoxyl N atoms to the Mn ion are Mn(1)···N(24) 9.740(4) and Mn(1)···N(54) 9.530(4) Å.

Table 3 Selected bond lengths (Å) and angles (°) for $[MnL^1_2][BF_4]_2 \cdot 1.5MeCN \cdot 0.25H_2O$ **1**·1.5MeCN·0.25H_2O

Mn(1)–N(2)	2.231(3)	Mn(1)–N(38)	2.188(3)
Mn(1)–N(8)	2.191(3)	Mn(1)–N(44)	2.249(3)
Mn(1)–N(14)	2.246(4)	N(24)–O(31)	1.284(5)
Mn(1)–N(32)	2.263(3)	N(54)–O(61)	1.281(5)
N(2)–Mn(1)–N(8)	72.6(1)	N(8)–Mn(1)–N(44)	110.6(1)
N(2)–Mn(1)–N(14)	144.7(1)	N(14)–Mn(1)–N(32)	92.4(1)
N(2)–Mn(1)–N(32)	98.3(1)	N(14)–Mn(1)–N(38)	109.4(1)
N(2)–Mn(1)–N(38)	105.9(1)	N(14)–Mn(1)–N(44)	96.3(1)
N(2)–Mn(1)–N(44)	94.2(1)	N(32)–Mn(1)–N(38)	72.4(1)
N(8)–Mn(1)–N(14)	72.2(1)	N(32)–Mn(1)–N(44)	144.5(1)
N(8)–Mn(1)–N(32)	104.8(1)	N(38)–Mn(1)–N(44)	72.2(1)
N(8)–Mn(1)–N(38)	176.7(1)		

The packing within the crystal lattice of complex **1** is of interest, since close N–O···H–C contacts between one aminoxyl moiety and the H atoms of a neighbouring molecule can mediate intermolecular magnetic interactions in solid aminoxyls.[17] In the lattice of **1**, O(61) forms contacts to two protons of a terpyridyl ring on an adjacent molecule related by the operation $1 + x, y, z$ [O(61)···H(6′) 2.26, O(61)···H(10′) 2.49 Å; Fig. 2]. However, O(31) exhibits an unusual mode of packing to a piperidinoxyl group of a molecule of symmetry $-1 - x, -y, -1 - z$. The closest contact of O(31) to this neighbour is to the aminoxyl O atom O(31″), rather than to a methyl hydrogen atom (Fig. 2), the O(31)···O(31″) distance being 3.543(5) Å. This is significantly greater than the 2.80 Å sum of the van der Waals radii of two O atoms, however. There is also an interaction between O(31) and a methyl proton from a lattice acetonitrile molecule [H(75C‴) of symmetry $-1 + x, -1 + y, z$], with O(31)···H(75C‴) 2.43 Å (Fig. 2).

Electrochemistry

Voltammetric data for L^1 and complexes **1**–**5** in MeCN–0.1 M $NBu^n_4PF_6$ at 293 K are summarised in Table 4. The cyclic voltammogram of L^1 exhibits a reversible oxidation at $E_{\frac{1}{2}} = +0.34$ V *vs.* the ferrocene–ferrocenium couple, corresponding to the one-electron oxidation of the aminoxyl moiety to an oxoammonium centre [equation (1)].[18]

$$R_2N{-}O^{\bullet} \longrightarrow R_2N{=}O^+ + e^- \qquad (1)$$

All complexes in the study show this couple as a fully reversible two-electron wave (by comparison with the peak currents shown by metal centred processes, see below), at $E_{\frac{1}{2}} = +0.37 \pm 0.01$ V (Fig. 3). This wave is chemically reversible at scan rates (ν) of 10–1000 m V^{-1} s, plots of I_p *vs.* $\nu^{\frac{1}{2}}$ giving straight lines. Importantly, the half-potential of this oxidation is the same for **2**, where the $Co^{II/III}$ couple is more negative than this L^1–$[L^1]^+$ process, as for **1** and **3**–**5**. Hence, varying the charge on the metal ion has no observable effect on the oxidation potential of the piperidinoxyl pendants in $[ML^1_2]^{n+}$ ($n = 2$ or 3) complexes. Compound L^1 also shows an irreversible reduction at $E_{p_c} = -2.03$ V, which we assign to a one-electron

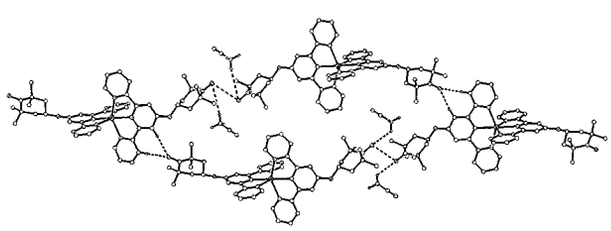

Fig. 2 Solid state structure of the $[MnL^1_2]^{2+}$ dication in **1**·1.5MeCN·0.25H_2O, showing the intermolecular contacts involving the piperidinoxyl groups. For clarity, the BF_4^- anions and solvent molecules not taking part in these interactions are not shown, while only hydrogen atoms attached to carbon atoms involved in intermolecular N–O···H–C interactions are included

Table 4 Cyclic voltammetric data for the compounds in this study. All voltammograms were run in MeCN–0.1M $NBu^n_4PF_6$ at 293 K. All data are quoted *vs.* ferrocene–ferrocenium couple, for a scan rate of 100 mV s^{-1}

Compound	L^1–$[L^1]^+$ couple $E_{\frac{1}{2}}$/V (ΔE_p/mV)	L^1–$[L^1]^-$ couple E_{pc}/V	M^{II}–M^{III} couple $E_{\frac{1}{2}}$/V (ΔE/mV)	M^{II}–M^{I} couple $E_{\frac{1}{2}}$/V (ΔE_p/mV)	M^{I}–M^{0} couple E_{pc}/V
L^1	+0.34 (88)	−2.03	—	—	—
1	+0.38 (110)	—	+1.43*	−1.30*	−1.90
2	+0.38 (104)	−2.21	−0.17 (90)	−1.32 (90)	−1.5 (sh)
3	+0.36 (71)	−2.13	+1.12 (71)	−1.69*	−1.98
4	+0.38 (83)	−2.21	—	−0.77*	−1.03
5	+0.37 (105)	−2.10	—	—	—

* Irreversible process, E_p value quoted.

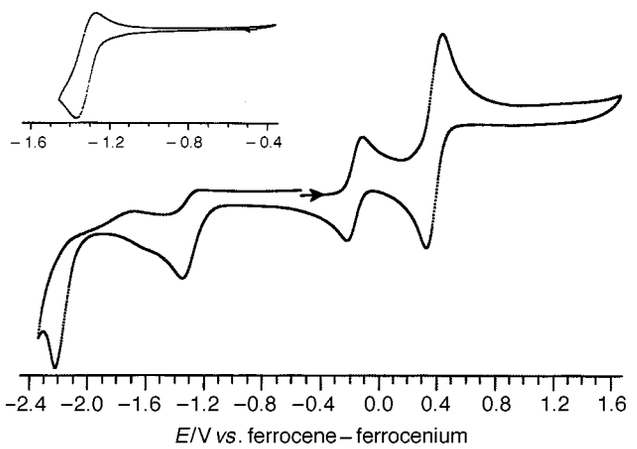

Fig. 3 Cyclic voltammogram of $[CoL^1_2][BF_4]_2$ **2** in MeCN–0.1 M $NBu^n_4PF_6$ at 293 K, scan rate 100 mV s^{-1}. Inset: the first reduction wave, showing its quasi-reversibility, scan rate 100 mV s^{-1}

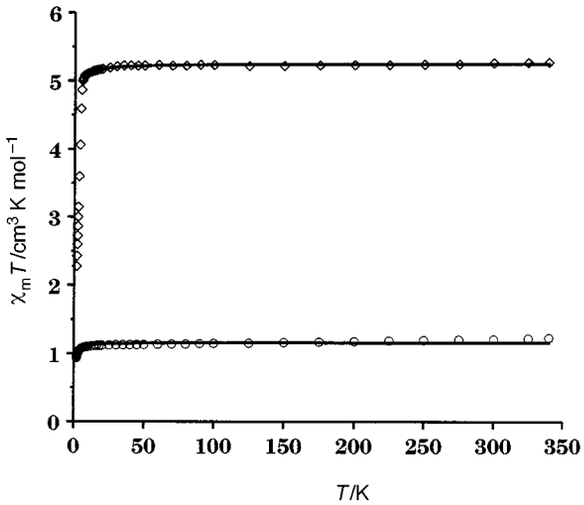

Fig. 4 Plots of X_mT *vs.* T for $[MnL^1_2][BF_4]_2$ **1** (◇) and $[CuL^1_2][BF_4]_2$ **4** (○). The solid lines represent fits of the data by the Curie-Weiss law; see text for details and fitting parameters

reduction of the terpyridyl π system (terpy is reduced irreversibly at $E_{p_c} = -2.4$ V in this solvent[19–21]). Complexes **1**–**5** also show an irreversible two-electron reduction at $E_{p_c} \approx -2.2$ V, ascribable to the reduction of co-ordinated L^1.

The metal-centred electrochemical behaviour of complexes **1**–**4** is complicated (Table 4). Compound **1** shows an irreversible one-electron oxidation at $E_{p_a} = +1.43$ V, with no associated daughter products, which we assign to a manganese(II)–manganese(III) oxidation, and broad irreversible reduction waves at $E_{p_c} = -1.30$ and -1.90 V. Scanning past the latter peak results in deposition of an unknown material (possibly manganese metal) onto the electrode, so that we tentatively assign these processes to $Mn^{II/I}$ and $Mn^{I/0}$ reductions. Similarly, **2** shows a reversible $Co^{II/III}$ couple at $E_{\frac{1}{2}} = -0.18$ V and a quasi-reversible $Co^{II/I}$ wave at $E_{\frac{1}{2}} = -1.32$ V (Fig. 3). The cathodic peak of this latter couple bears an irreversible high-potential shoulder close to -1.5 V, which may correspond to a $Co^{I/0}$ process; scanning past this potential causes disappearance of the $Co^{I/II}$ return wave. Complex **3** shows a reversible $Ni^{II/III}$ couple at $E_{\frac{1}{2}} = +1.12$ V, and irreversible reductions at $E_{p_c} = -1.69$ and -1.98 V that may be assigned as $Ni^{II/I}$ and $Ni^{I/0}$ processes.

The $M^{II/III}$ waves exhibited by complexes **1**–**3** occur at comparable potentials to those shown by other $[M(terpy)_2]^{2+}$ (M = Mn,[19,21,22] Co[21–23] or Ni[21,22,24]) derivatives in MeCN. However, the reductive behaviour of **1**–**3** contrasts with that previously reported for this class of compounds, which all exhibit reversible $M^{II/I}$ and $M^{I/0}$ couples (although the assignment of the putative $M^{I/0}$ reductions in these studies is uncertain), at half-potentials that vary only slightly upon substitution at the 4′ position of the terpy ligands but are significantly different from those shown by **1**–**3**.[19,21–24] Unfortunately, the irreversibility of the reductive metal-centred processes exhibited by **1**–**3** has precluded any more detailed experiments to confirm our suggested assignments. Interestingly, the irreversible $Cu^{II/I}$ and $Cu^{I/0}$ reductions of **4** (Table 4) occur at essentially identical potentials to those previously described for other $[Cu(terpy)_2]^{2+}$ complexes.[21,25]

EPR and magnetic studies

The X-band EPR spectra of complexes **1**–**5** at 293 K in MeCN–toluene (10:1) exhibit a weak three-line signal attributable to deco-ordinated L^1. For **1**–**3** and **5** no other EPR signals were detected. However, **4** also exhibits a much more intense, broad featureless line centred at $\langle g \rangle = 2.04$, together with a very weak half-field resonance close to 1590 G, both of which are attributable to the $[CuL^1_2]^{2+}$ complex. An identical spectrum was observed at Q-band. The unresolved resonance observed for **4** implies that the Cu/L^1 superexchange constant $|J| \geqslant (\langle g \rangle_{Cu} - \langle g \rangle_{L^1})$. In this case, the g value for **4** is described by equation (2). Since $[Cu(terpy)_2]^{2+}$ shows $\langle g \rangle = 2.13$ under our

$$\langle g \rangle_{obs} = [2\langle g \rangle(L^1) + \langle g \rangle(Cu)]/3 \qquad (2)$$

conditions,[11,13] and $\langle g \rangle = 2.006$ for L^1, this gives a calculated $\langle g \rangle_{obs} = 2.05$ for **4**, in good agreement with the observed value. We can therefore estimate that $|J| \geqslant 0.07$ cm^{-1}, from the Q-band measurements. This is a high value for a copper(II) complex of a 2,2,6,6-tetramethylpiperidin-1-oxyl substituted pyridine,[5] but is an identical result to that obtained for $[CuL^2_4][BF_4]_2$.[7]

Variable temperature magnetic susceptibility measurements were performed on dried powder samples of complexes **1** and **4** (Fig. 4, SUP 57399). Susceptibility data for **1** show that between 10 and 340 K χ_mT is constant at 5.2 cm^3 K mol^{-1}, which is in excellent agreement with the spin-only value for non-interacting $S = \frac{5}{2}$ and two $S = \frac{1}{2}$ spins (5.13 cm^3 K mol^{-1} with $g = 2.00$); below 10 K, χ_mT decreases rapidly, to 2.3 cm^3 K mol^{-1} at 1.8 K. Data for $T \geqslant 5$ K were well reproduced by the Curie–Weiss law, giving $g = 2.02$ and $\theta = -0.3$ K; attempted fits of all data were not satisfactory, however. A model describing intramolecular superexchange within a linear three-spin system was therefore derived by the Kambe method,[26] according to the Hamiltonian in equation (3). Here, S_1 corresponds to the metal ion of the

$$\mathscr{H} = -2J(S_1 \cdot S_2 + S_1 \cdot S_3) - 2J'(S_2 \cdot S_3) \qquad (3)$$

$[ML^1_2]^{2+}$ complex (M = Mn for **1**), and S_2 and S_3 to the two L^1 aminoxyl spins. However, this model did not reproduce the low-temperature behaviour of **1** any more successfully than the Curie–Weiss equation.

The dominant antiferromagnetism observed for complex **1** is surprising, since precedent suggests that intramolecular metal/aminoxyl superexchange in manganese(II) complexes of spin-labelled pyridines should be ferromagnetic.[27] However, the shape of the χ_mT *vs.* T curve for **1** (plateau until very low T, followed by a sharp decline; Fig. 4) is suggestive of competing ferro- and antiferro-magnetic contributions. In addition, the inability of the Curie–Weiss equation to model the data is consistent with the presence of an efficient intermolecular superexchange pathway in solid **1**, that survives loss of crystallinity upon drying. We tentatively propose, therefore, that the

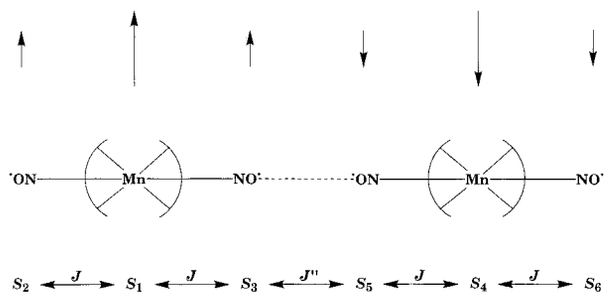

Scheme 1 Suggested magnetic coupling scheme for complex **1**, showing the origin of the proposed $S = 0$ ground state; S_1 and S_4 are $S = \frac{5}{2}$ manganese(II) centres, while S_2, S_3, S_5 and S_6 are L^1 aminoxyl spins. For clarity the constant J', describing superexchange between S_2 and S_3, and S_5 and S_6 [equation (3)], has been omitted since it is expected that $J, J'' \gg J'$

data reflect the unusual O···O contacts between pairs of $[MnL^1_2]^{2+}$ dications in crystalline **1** (Fig. 2, Scheme 1). Weak ferromagnetic Mn/aminoxyl coupling [J in Scheme 1 and equation (3)] would then be balanced by an antiferromagnetic intradimer intermolecular interaction (J''), to give an overall $S = 0$ ground state for the dimeric unit. However, the resultant six-spin system cannot be solved by the Kambe approach, so this suggestion remains to be verified.

Susceptibility data for complex **4** show that between 5 and 340 K $\chi_m T$ is effectively constant within the range 1.1–1.2 cm^3 K mol^{-1}, which again compares well with the spin-only value for three non-interacting $S = \frac{1}{2}$ centres (1.14 cm^3 K mol^{-1} with $g = 2.00$). Below 5 K there is a small decrease in $\chi_m T$, to 0.9 cm^3 K mol^{-1} at 1.8 K. In contrast to **1**, all data for **4** could be fitted with the Curie–Weiss law, giving $g = 2.03$ and $\theta = -0.4$ K. A model describing intramolecular superexchange for **4** based on equation (3) (M = Cu) was also derived.[26,27] Fixing g (L^1) = 2.01, this model also reproduced the data well with g(Cu) = 2.07, although J and J' were strongly correlated. Since J should be $\gg J'$ in this model, a fit of the data with $J' = 0$ was performed giving g(Cu) = 2.07 and $J = -0.4$ cm^{-1}.

The weakness of the antiferromagnetic interactions in complex **4** makes it impossible to determine J accurately, or to be certain whether equation (3) properly represents the magnetic behaviour of this compound. However, given the identical EPR properties shown by **4** and $[CuL^2_4][BF_4]_2$, it is suggestive that the solid state magnetic behaviour of the latter compound is also essentially identical to that of **4**.[7] In addition, previous work has shown that intramolecular Cu/aminoxyl superexchange in copper(II) complexes of 2,2,6,6-tetramethylpiperidin-1-oxyl substituted pyridines is usually antiferromagnetic.[5] It is therefore likely that the antiferromagnetic interactions in both powdered **4** and $[CuL^2_4][BF_4]_2$ derive predominantly from intramolecular superexchange.

Experimental

All manipulations were performed in air using commercial grade solvents. 4′-Chloro-2,2′:6′,2″-terpyridine, 4-hydroxy-2,2,6,6-tetramethylpiperidin-1-oxyl, $Cu(BF_4)_2 \cdot xH_2O$ ($x \approx 4$; Aldrich), $AgBF_4$, $Mn(O_2CMe)_2 \cdot 4H_2O$, $Co(O_2CMe)_2 \cdot 4H_2O$, $Ni(BF_4)_2 \cdot 6H_2O$ and $ZnCl_2$ (Avocado) were used as supplied. Analytical and UV/VIS data for the compounds are summarised in Tables 1 and 2.

Syntheses

2,2,6,6-Tetramethyl-4-(2,2′:6′,2″-terpyridin-4′-yloxy)-piperidin-1-oxyl (L^1). To a suspension of freshly ground KOH (2.64 g, 4.72×10^{-2} mol) in dmso (35 cm^3) was added 4-hydroxy-2,2,6,6-tetramethylpiperidin-1-oxyl (2.00 g, 1.18×10^{-2} mol), followed by 4′-chloro-2,2′:6′,2″-terpyridine (3.33 g, 1.18×10^{-2} mol). The mixture was stirred at 50 °C for 16 h, then quenched with an equal volume of water to afford a pink solid which was dried over P_2O_5. Recrystallisation from hot hexanes gave feathery pale pink needles. Yield 3.5 g, 74%. M.p. 128–130 °C. ^{1}H NMR spectrum (CD_3CN, 293 K): δ 8.7 (4 H, terpy $H^{6/6''}$ + $H^{3/3''}$), 8.3 (2 H, terpy $H^{3'/5'}$), 7.9 (2 H, terpy $H^{4/4''}$) and 7.1 (2 H, terpy $H^{5/5''}$).

Bis[2,2,6,6,-tetramethyl-4-(2,2′:6′,2″-terpyridin-4′-yloxy)-piperidin-1-oxyl]manganese(II) bis(tetrafluoroborate) 1. Compound L^1 (0.20 g, 4.96×10^{-4} mol), $Mn(O_2CMe)_2 \cdot 4H_2O$ (0.061 g, 2.48×10^{-4} mol) and $NaBF_4$ (0.055 g, 4.96×10^{-4} mol) were allowed to react in MeCN (20 cm^3) at room temperature for 30 min, giving a yellow solution and white NaCl precipitate. The solution was filtered and concentrated to *ca.* 2 cm^3 volume. Vapour diffusion of Et_2O into this solution afforded yellow platelets, which were dried *in vacuo*. Yield 0.14 g, 55%.

Bis[2,2,6,6,-tetramethyl-4-(2,2′:6′,2″-terpyridin-4′-yloxy)-piperidin-1-oxyl]cobalt(II) bis(tetrafluoroborate) 2. Method as for **1**, using $Co(O_2CMe)_2 \cdot 4H_2O$ (0.061 g, 2.48×10^{-4} mol). The product formed brick red microcrystals from MeCN–Et_2O. Yield 0.16 g, 62%.

Bis[2,2,6,6,-tetramethyl-4-(2,2′:6′,2″-terpyridin-4′-yloxy)-piperidin-1-oxyl]nickel(II) bis(tetrafluoroborate) 3. A mixture of L^1 (0.20 g, 4.96×10^{-4} mol) and $Ni(BF_4)_2 \cdot 6H_2O$ (0.084 g, 2.48×10^{-4} mol) was stirred in MeCN (20 cm^3) at room temperature for 15 min. The resultant tan solution was reduced to *ca.* 3 cm^3 volume, whereupon a tan solid slowly precipitated. An equal volume of Et_2O was added, and the mixture stored at −30 °C. After filtration, the solid was recrystallised from $MeNO_2$–Et_2O to yield tan microcrystals, which were dried *in vacuo*. Yield 0.14 g, 54%.

Bis[2,2,6,6,-tetramethyl-4-(2,2′:6′,2″-terpyridin-4′-yloxy)-piperidin-1-oxyl]copper(II) bis(tetrafluoroborate) 4. A solution of L^1 (0.20 g, 4.96×10^{-4} mol) and $Cu(BF_4)_2 \cdot xH_2O$ (0.077 g, 2.48×10^{-4} mol) in MeCN (20 cm^3) at room temperature for 15 min, gave a green solution that was then concentrated to *ca.* 2 cm^3 volume. Vapour diffusion of Et_2O into this solution yielded fine pale green needles, which were dried *in vacuo*. Yield 0.18 g, 70%.

Bis[2,2,6,6,-tetramethyl-4-(2,2′:6′,2″-terpyridin-4′-yloxy)-piperidin-1-oxyl]zinc(II) bis(tetrafluoroborate) 5. Method as for **1**, using $ZnCl_2$ (0.034 g, 2.48×10^{-4} mol). The product formed pale orange microcrystals from MeCN–Et_2O. Yield 0.18 g, 70%. ^{1}H NMR spectrum (CD_3CN, 293 K): δ 8.7 (4 H, terpy $H^{6/6''}$ + $H^{3/3''}$), 8.3 (2 H, terpy $H^{3'/5'}$), 8.0 (2 H, terpy $H^{4/4''}$) and 7.4 (2 H, terpy $H^{5/5''}$).

Crystallography

Vapour diffusion of Et_2O into dilute MeCN solutions of complex **1** afforded yellow plates. Experimental details for the structure determination are given in Table 5. The structure was solved by direct methods (SHELXTL PLUS[28]) and refined by full matrix least squares on F^2 (SHELXL 93[29]). During refinement, one of the BF_4^- anions was found to be disordered, and was modelled with partial fluorine site occupancies such that the total number of F atoms equalled 4. Two molecules of lattice MeCN were located; one of these [C(75)–N(77)] was fully occupied, but the other [C(78)–N(80)] was given an occupancy of 0.5. In addition, a weakly scattering feature that was bonded to no other atom was modelled as 0.25 of a molecule of water. All non-H atoms with occupancies ≥0.5 were refined anisotropically, and H atoms were placed in calculated positions. No restraints were applied.

Table 5 Experimental details for the single crystal structure determination of $[MnL^1_2][BF_4]_2 \cdot 1.5MeCN \cdot 0.25H_2O$ **1**·1.5MeCN·0.25H_2O

Formula	$C_{51}H_{58.5}B_2F_8MnN_{9.5}O_{4.25}$
M_r	1101.13
Crystal class	Triclinic
Space group	$P\bar{1}$ (no.2)
a/Å	17.403(3)
b/Å	18.906(4)
c/Å	9.077(2)
α/°	90.68(2)
β/°	93.29(2)
γ/°	114.11(1)
u/Å^3	2720(1)
Z	2
μ(Mo-Kα)/mm^{-1}	0.323
T/K	150(2)
Measured reflections	8834
Independent reflections	8514
R_{int}	0.030
$R(F)$	0.064
$wR(F^2)$	0.191
Goodness of fit	1.052

$R = \Sigma[|F_o| - |F_c|]/\Sigma|F_o|$, $wR = [\Sigma w(F_o^2 - F_c^2)/\Sigma wF_o^4]^{\frac{1}{2}}$.

CCDC reference number 186/1035.

See http://www.rsc.org/suppdata/dt/1998/2477/ for crystallographic files in .cif format.

Other measurements

Infrared spectra were obtained as Nujol mulls pressed between KBr windows between 400 and 4000 cm^{-1} using a Perkin-Elmer Paragon 1000 spectrophotometer, and UV/VIS spectra with a Perkin-Elmer Lambda 12 spectrophotometer operating between 200 and 1100 nm, in 1 cm quartz cells. All ^{1}H NMR spectra were run on a Bruker DPX250 spectrometer, operating at 250.1 MHz. Positive ion fast atom bombardment (FAB) mass spectra were performed on a Kratos MS890 spectrometer, employing a 3-nitrobenzyl alcohol matrix. Microanalyses (C, H, N) were performed by the University of Cambridge Department of Chemistry microanalytical service. Melting points are uncorrected. The EPR spectra were obtained using a Bruker ESP300E spectrometer; X-band spectra employed a ER4102ST resonator and ER4111VT cryostat, while for Q-band spectra a ER5106QT resonator and an ER4118VT cryostat were used. All electrochemical measurements were carried out using an Autolab PGSTAT20 voltammetric analyser, in MeCN containing 0.1 M $NBu^n_4PF_6$ (prepared from NBu^n_4OH and HPF_6) as supporting electrolyte. Cyclic voltammetric experiments involved the use of a double platinum working/counter electrode and a silver wire reference electrode; all potentials are referenced to a ferrocene–ferrocenium standard. Variable temperature magnetic susceptibility measurements were obtained using a Quantum Design SQUID magnetometer in an applied field of 1000 G. Diamagnetic corrections for the samples were estimated from Pascal's constants;[30] diamagnetic corrections for the sample holders were also applied. Observed and calculated data were refined using SIGMAPLOT.[31]

Acknowledgements

The authors thank the Royal Society (University Research Fellowship to M. A. H.), the EPSRC (E. K. B.), the University of Cambridge and St. Catharine's College for financial support.

References

1 M. F. Ottaviani, N. D. Ghatlia and N. J. Turro, *J. Phys. Chem.*, 1992, **96**, 6075; M. F. Ottaviani, C. Turro, N. J. Turro, S. H. Bossmann and D. A. Tomalia, *J. Phys. Chem.*, 1996, **100**, 13 667.
2 M. F. Ottaviani, N. D. Ghatlia, S. H. Bossmann, J. K. Barton, H. Dürr and N. J. Turro, *J. Am. Chem. Soc.*, 1992, **114**, 8946.
3 S. H. Bossmann, N. D. Ghatlia, M. F. Ottaviani, C. Turro, H. Dürr and N. J. Turro, *Synthesis*, 1996, 1313.
4 J.-P. Sauvage, J.-P. Collin, J.-C. Chambron, S. Guillerez, C. Coudret, V. Balzani, F. Barigeletti, L. De Cola and L. Flamigni, *Chem. Rev.*, 1994, **94**, 993; E. C. Constable, *Prog. Inorg. Chem.*, 1994, **42**, 67; A. Harriman and R. Ziessel, *Chem. Commun.*, 1996, 1707; E. C. Constable, *Pure Appl. Chem.*, 1996, **68**, 253; F. Barigeletti, L. Flamigni and J.-P. Collin, *Chem. Commun.*, 1997, 333; E. C. Constable, *Chem. Commun.*, 1997, 1073.
5 S. S. Eaton and G. R. Eaton, *Coord. Chem. Rev.*, 1978, **26**, 207; 1988, **83**, 29.
6 G. R. Newkome, F. Cardullo, E. C. Constable, C. N. Moorefield and A. M. W. Cargill Thompson, *J. Chem. Soc., Chem. Commun.*, 1993, 925; D. Armspach, M. Cattalini, E. C. Constable, C. E. Housecroft and D. Phillips, *Chem. Commun.*, 1996, 1823; G. R. Newkome and E. He, *J. Mater. Chem.*, 1997, **7**, 1237.
7 M. A. Halcrow, L. M. Rodriguez-Martinez, E. K. Brechin, J. E. Davies, I. J. Scowen and M. McPartlin, *J. Organomet. Chem.*, in the press.
8 R. P. Thummel and Y. Jahng, *J. Org. Chem.*, 1985, **50**, 2407.
9 A. R. Forster, J. M. Hay and R. H. Thomson, *Organic Chemistry of Stable Free Radicals*, Academic Press, New York, 1968; ch. 5, pp. 180–246; E. G. Rozantsev and V. D. Sholle, *Synthesis*, 1971, 190; J. F. W. Keana, *Chem. Rev.*, 1978, **78**, 37.
10 R. Briere, H. Lemaire, H. Rassat, P. Rey and A. Rousseau, *Bull. Soc. Chim. Fr.*, 1967, 4479; R. Briere, H. Lemaire, H. Rassat and J.-J. Dunand, *Bull. Soc. Chim. Fr.*, 1970, 4220.
11 W. Henke and D. Reinen, *Z. Anorg. Allg. Chem.*, 1977, **436**, 187.
12 A. J. Baker, D. C. Craig and A. D. Rae, *Aust. J. Chem.*, 1995, **48**, 1373.
13 J.-V. Folgado, W. Henke, R. Allmann, H. Stratemeier, D. Beltrán-Porter, T. Rojo and D. Reinen, *Inorg. Chem.*, 1990, **29**, 2035.
14 S. Kremer, W. Henke and D. Reinen, *Inorg. Chem.*, 1982, **21**, 3013.
15 R. Bhula and D. C. Weatherburn, *Aust. J. Chem.*, 1991, **44**, 303.
16 B. N. Figgis, E. S. Kucharski and A. H. White, *Aust. J. Chem.*, 1983, **36**, 1537.
17 T. Nogami, T. Ishida, M. Yasui, F. Iwasaki, N. Takeda, M. Ishikawa, T. Kawagami and K. Yamaguchi, *Bull. Chem. Soc. Jpn.*, 1996, **69**, 1841.
18 W. Sümmermann and U. Deffner, *Tetrahedron*, 1975, **31**, 593.
19 S. Musumeci, E. Rizzarelli, S. Sammartano and R. P. Bonomo, *J. Electroanal. Chem., Interfacial Electrochem.*, 1973, **46**, 109; J. M. Rao, M. C. Hughes and D. J. Macero, *Inorg. Chim. Acta*, 1976, **16**, 231; J. M. Rao, D. J. Macero and M. C. Hughes, *Inorg. Chim. Acta*, 1980, **41**, 221.
20 E. C. Constable, J. Lewis, M. C. Liptrot and P. R. Raithby, *Inorg. Chim. Acta*, 1990, **178**, 47.
21 G. D. Storrier, S. B. Colbran and D. C. Craig, *J. Chem. Soc., Dalton Trans.*, 1998, 1351.
22 C. Arana, M. Kesharvaz, K. T. Potts and H. D. Abruña, *Inorg. Chim. Acta*, 1994, **225**, 285.
23 J. M. Rao, M. C. Hughes and D. J. Macero, *Inorg. Chim. Acta*, 1976, **18**, 127; M. C. Hughes, D. J. Macero and J. M. Rao, *Inorg. Chim. Acta*, 1981, **49**, 241.
24 M. Aihara, H. Kishita and S. Misumi, *Bull. Chem. Soc. Jpn.*, 1975, **48**, 680; R. Prasad and D. B. Scaife, *J. Electroanal. Chem., Interfacial Electrochem.*, 1977, **84**, 373.
25 A. L. Crumbliss and A. T. Poulos, *Inorg. Chem.*, 1975, **14**, 1529; K. T. Potts, M. Kesharvaz-K, F. S. Tham, H. D. Abruña and C. Arana, *Inorg. Chem.*, 1993, **32**, 4450.
26 K. Kambe, *J. Phys. Soc. Jpn.*, 1950, **5**, 48.
27 A. Caneschi, F. Ferraro, D. Gatteschi, P. Rey and R. Sessoli, *Inorg. Chem.*, 1990, **29**, 4217.
28 G. M. Sheldrick, SHELXTL PLUS, PC version, Siemens Analytical Instruments Inc., Madison, WI, 1990.
29 G. M. Sheldrick, SHELXL 93, University of Göttingen, 1993.
30 C. J. O'Conner, *Prog. Inorg. Chem.*, 1982, **29**, 203.
31 SIGMAPLOT, version 5.0.1, Jandel Scientific, Erkrath, 1996.

Received 20*th May* 1998; *Paper* 8/03793K